

Electrostatic potential profiles of molecular conductors

G. C. Liang,* A. W. Ghosh,† M. Paulsson, and S. Datta

School of Electrical and Computer Engineering, Purdue University, W. Lafayette, IN 47907

(Dated: October 22, 2018)

The electrostatic potential across a short ballistic molecular conductor depends sensitively on the geometry of its environment, and can affect its conduction significantly by influencing its energy levels and wave functions. We illustrate some of the issues involved by evaluating the potential profiles for a conducting gold wire and an aromatic phenyl dithiol molecule in various geometries. The potential profile is obtained by solving Poisson's equation with boundary conditions set by the contact electrochemical potentials and coupling the result self-consistently with a nonequilibrium Green's function (NEGF) formulation of transport. The overall shape of the potential profile (ramp vs. flat) depends on the feasibility of transverse screening of electric fields. Accordingly, the screening is better for a thick wire, a multiwalled nanotube or a close-packed self-assembled monolayer (SAM), in comparison to a thin wire, a singlewalled nanotube or an isolated molecular conductor. The electrostatic potential further governs the alignment or misalignment of intramolecular levels, which can strongly influence the molecular I-V characteristic. An external gate voltage can modify the overall potential profile, changing the current-voltage (I-V) characteristic from a resonant conducting to a saturating one. The degree of saturation and gate modulation depends on the availability of metal-induced-gap states (MIGS) and on the electrostatic gate control parameter set by the ratio of the gate oxide thickness to the channel length.

PACS numbers: PACS numbers: 85.65.+h, 73.23.-b, 31.15.Ar

Recently there has been considerable progress in the experimental analysis [1, 2, 3, 4] and theoretical modeling [5, 6, 7, 8, 9] of molecular electronic devices. Conduction through a molecule depends on its intrinsic chemistry, as well as external influences such as the electrode geometry, charging and bonding at the electrodes. In particular, the electrostatic potential profile in molecular devices is a quantity of great interest, because it contributes to the self-consistent field in the molecular Hamiltonian, thereby influencing the electronic properties and regulating the flow of current. The spatial variation of the electrostatic potential carries nontrivial information about molecular screening, the presence of impurities and Schottky barriers, as well as features related to the alignment of energy levels within the molecule [10, 11]. Furthermore, the long-ranged nature of electrostatic forces allows the molecular levels and wavefunctions to be tuned remotely, with a gate electrode for example.

It is often stated that the voltage drop in a ballistic conductor needs no discussion, for all the drop must be localized at the interfaces with the contacts. While this is true in some sense for the *electrochemical potential profile*, $\mu(\vec{r})$, it is certainly not true for the *electrostatic potential*, $\phi(\vec{r})$; in fact, the two profiles can differ widely in low-dimensional materials with long screening lengths. We will try to bring out this distinction later using a simple classical diffusion model, since $\mu(\vec{r})$ is a tricky concept to define under more general conditions of transport. The electrostatic potential $\phi(\vec{r})$, by contrast, is a clearly defined concept even for quantum transport far from equilibrium. This paper is essentially about $\phi(\vec{r})$. Under certain conditions the electrostatic potential profile can

have significant effects on the current-voltage characteristics of a conductor [12]. In a standard two-terminal molecular conductance measurement [1, 2], for example, the precise division of the applied bias between the source and drain contacts can cause the I-V to change from symmetric to asymmetric, with the conductance gap determined either by the molecular levels exclusively or by the contact Fermi energy in addition [13]. Such a sensitive dependence of current conduction on the potential profile is not typical in mesoscopic physics, but quite routine in molecular electronics. We will try to provide simple insights to describe such conditions.

Direct measurement of the electrostatic potential profile of a molecular conductor is challenging, given its small size. Attempts at direct AFM-based or potentiometric measurement of the profile have been limited to long ($\sim 0.3 - 3 \mu\text{m}$) carbon nanotubes [14] or organic molecular solids [15], where the profile has been determined mainly to be flat inside the molecular system, with the voltage drop largely occurring at the contacts. Similar profiles have been theoretically postulated or invoked in various semi-empirical treatments of molecular conduction [5, 12]. In sharp contrast, a ramp-like potential across a molecular wire has been calculated by semi-empirical [16], as well as a number of first-principles density functional theory (DFT)-based simulations [6, 7, 8]. It is further reasonable to expect that potential variations on an atomic scale would be influenced by atomistic features on the contacts and surrounding molecules. The nature of the potential profile thus needs to be sorted out.

In this paper we perform a fully quantum kinetic, atomistic treatment of the electrostatic potential profile



FIG. 1: Schematic of two-terminal geometry, with metal contacts of infinite cross section coupled to an active device. The device will be replaced by a gold wire of various shapes throughout the rest of the paper, and by a phenyl dithiol (PDT) molecule towards the end. Part of the contact material may be included in the device in addition.

across a prototype molecular conductor, and examine its influence on experimentally measurable current-voltage (I-V) characteristics of the conductor. The prototype conductor we investigate is either a gold atomic chain or a phenyl dithiol molecule, attached to a cluster of metal atoms on both ends and sandwiched between metal contacts of infinite cross section (Fig. 1). The “trivial” Laplace part ϕ_L of the potential profile depends on the geometry and dielectric constants of the molecule and the electrodes. This part is expected to dominate the electronic properties for insulators and molecular conductors away from resonance, and can be modulated externally with a gate, leading potentially to transistor action. Furthermore, the Laplace part determines the alignment of energy levels localized on different parts of the molecule, which could drive interesting quantum effects such as current rectification or negative differential resistance (NDR). In contrast, the quantum contributions to the potential through the Poisson term $\phi_p(\rho)$ are affected by the atomicity of the device. The Poisson part becomes important in conducting systems such as metallic wires, metallic nanotubes and molecules driven into resonance with a source-drain bias or turned on with a gate. $\phi_p(\rho)$ contains nontrivial physics, including self-consistent charging, screening and Friedel oscillations.

Section I provides a semiclassical description of conduction that outlines the difference between the electrochemical and the electrostatic potentials. Section II describes the nonequilibrium transport formalism that we employ, and the model geometries and Hamiltonians that we use. Section III calculates the voltage drop within the contacts, illustrating that only a fraction of the applied bias drops across a charge neutral region including the molecule and the contacts. Section IV discusses the dependence of the potential profile on the thickness of the wire, specifically addressing the feasibility of adequate amount of transverse screening. Similar issues related to ineffective screening in 1-D have been raised in the context of carbon nanotubes [17]. Section V addresses the importance of screening by the environment, such as in a self-assembled monolayer (SAM) of molecular wires.

In section VI we look at potential variations within the molecule, which although small could nevertheless significantly influence observable electronic properties, such as the current-voltage (I-V) characteristics. Finally in Section VII, we talk about the influence of remote contacts such as a gate electrode on the potential profile, which in turn determines three-terminal transistor I-Vs. We summarize our results in section VIII.

I. SEMICLASSICAL DESCRIPTION OF POTENTIAL PROFILE

In this section, we present a simplified semiclassical, continuum description of current conduction, invoking macroscopic parameters such as the conductivity tensor and the dielectric constant. The aim of this section is to provide an elementary description of the distinction between electrochemical and electrostatic potentials. For molecular systems one cannot use such a macroscopic description, and a proper quantum kinetic description needs to be invoked (section II).

A semiclassical description involves defining a conductivity tensor $\sigma(\vec{r})$. The electrochemical potential satisfies the *equation of continuity*, while the electrostatic potential satisfies *Poisson's equation*:

$$\vec{\nabla} \cdot (\sigma \vec{\nabla} \mu) = 0 \quad (1a)$$

$$\vec{\nabla} \cdot (\epsilon \vec{\nabla} \phi) = -e^2 [n(\vec{r}) - N_D] \quad (1b)$$

where ϵ is the dielectric constant, N_D is the dopant density, and $n(\vec{r})$ is the electron density:

$$n(\vec{r}) = \int dE D(E, \vec{r}) f_0(E + \phi(\vec{r}) - \mu(\vec{r}))$$

$$f_0(E) = [1 + \exp(E/k_B T)]^{-1}, \quad (2)$$

$D(E, \vec{r})$ representing the local electron density of states (LDOS). A conductivity mismatch at the device-contact interfaces, such as that generated by a variation in the cross-sectional geometry or the doping profile, allows us to hold the contact electrochemical potentials at fixed voltages under bias, dropping μ almost entirely at the interfaces for a ballistic device [18]. This variation $\delta\mu$ influences the local charge distribution $\delta n(\vec{r})$ through the chemical potential $\mu - \phi$ (Eq. 2), so that the electrochemical potential profile $\mu(\vec{r})$ in effect acts as the driving force for the electrostatic potential profile $\delta\phi$ in Eq. 1b. In linear response, $\delta n(\vec{r}) \approx D_0 (\delta\mu - \delta\phi)$, where D_0 is the density of states (DOS) at the Fermi energy. Poisson's equation (1b) then reads:

$$\left(\nabla^2 - \frac{e^2 D_0}{\epsilon} \right) \delta\phi = -\frac{e^2 D_0}{\epsilon} \delta\mu \quad (3)$$

indicating that $\delta\phi$ is given by a convolution of $\delta\mu$ and a screening function that varies on a Debye (Thomas-Fermi) lengthscale given by $\lambda_D \approx \sqrt{\epsilon/e^2 D_0}$ [19]. (An

analogous expression can be invoked to describe screening by surface states [20]). *The electrostatic potential thus has a slower spatial variation than the electrochemical potential profile* [21]. In metallic conductors with a high DOS and correspondingly small Debye length the two profiles track each other in order to avoid large charge buildups. In contrast in a semiconductor or insulator having small DOS inside the bandgap the Debye length can be quite large, so that the two potentials can vary on widely different length scales [22]. A molecular conductor is intermediate between the two limits, acting as an insulator when the contact electrochemical potentials are off-resonant with the levels, and as a conductor on-resonance. One can thus have a nontrivial electrostatic potential profile even in a ballistic molecular device where the electrochemical potential does not vary spatially at all, except at the contact-molecular interfaces.

Having illustrated the basic distinction between the two kinds of voltage-drop, we now move onto a rigorous quantum kinetic and atomistic description of it.

II: QUANTUM KINETIC FORMALISM

Basic equations. Eq. 1a needs to be modified to solve for the full quantum transport under bias. At equilibrium, one could still use the concept of an electrochemical potential, defined by the contact Fermi energy E_F . The electronic local density of states (LDOS) are obtained by solving Schrödinger's equation for the molecular Hamiltonian, supplemented by a self-consistent potential U_{SCF} , and filling the eigenstates according to equilibrium statistical mechanics:

$$\begin{aligned} [H + U_{\text{SCF}}] \Psi_\alpha(\vec{r}) &= E_\alpha \Psi_\alpha(\vec{r}) \\ n_{\text{eq}}(\vec{r}) &= \sum_\alpha n_\alpha(\vec{r}) = \sum_\alpha |\Psi_\alpha(\vec{r})|^2 f_0(E_\alpha - E_F). \end{aligned} \quad (4)$$

In general, the self-consistent potential U_{SCF} consists of a Hartree-term obtained from the electrostatic potential ϕ that is the solution to Poisson's equation 1b with n replaced by n_{eq} , and additional exchange-correlation contributions that need to be incorporated through an appropriate ab-initio technique. The expression for n can be recast in the form Eq. 2 by recognizing that the LDOS $D(E, \vec{r}) = \sum_\alpha |\Psi_\alpha(\vec{r})|^2 \delta(E - E_\alpha)$.

Under bias, the contact electrochemical potentials separate, and the system is driven out of equilibrium in its bid to equilibrate with both contacts, causing a current flow. Under these nonequilibrium conditions an unambiguous common electrochemical potential is hard to define. One could, however, describe transport in terms of *groups* of electrons that are separately in equilibrium with the two contacts [18]. Furthermore, the contacts could fill the energy levels in a correlated way, so that one needs to deal with the full nonequilibrium density

matrix $\rho(\vec{r}, \vec{r}')$ of which the electron densities $n_\alpha(\vec{r})$ form just the diagonal parts. A formal way of handling these issues is by using the nonequilibrium Green's function (NEGF) prescription [18].

In the NEGF formalism, one deals with retarded, advanced, lesser and greater single-particle Green's functions [18]. The retarded Green's function matrix is

$$G(E) = [ES - H - U_{\text{scf}}(\rho) - \Sigma_S(E) - \Sigma_D(E)]^{-1}. \quad (5)$$

where H is the single-particle molecular Hamiltonian in an appropriate basis set, S is the overlap matrix in that basis-set, the self-consistent potential U_{scf} is dominated by the electrostatic potential ϕ (and in principle, includes exchange-correlation effects too), and the self-energy matrices $\Sigma_{S,D}$ represent the influence of scattering by the source (S) and drain (D) contacts. The contact self-energies can be calculated for electrodes of given geometry and surface bonding [6], yielding level broadenings $\Gamma_{S,D}$:

$$\Gamma_{S,D} = i \left[\Sigma_{S,D} - \Sigma_{S,D}^\dagger \right]. \quad (6)$$

The nonequilibrium density matrix ρ determining $\phi(\rho)$ is calculated self-consistently within the NEGF formalism using the lesser Green's function as [6, 18]:

$$\rho = \int dE [-iG^<(E)/2\pi], \quad (7)$$

with the electron density representing its diagonal component (see Eq. 12). The function $-iG^<(E)$ describes how the molecular states are filled in a correlated way by the two contacts, and is itself determined by the retarded Green's function G (Eq. 5), the broadenings $\Gamma_{S,D}$, and the contact electrochemical potentials $\mu_{S,D}$:

$$\begin{aligned} -iG^< &= G [f_S \Gamma_S + f_D \Gamma_D] G^\dagger \\ f_{S,D}(E) &= \left(1 + \exp \left[\frac{E - \mu_{S,D}}{k_B T} \right] \right)^{-1}. \end{aligned} \quad (8)$$

Since we *explicitly* include any asymmetry in electrostatic coupling with the contacts through $\phi(\rho)$ and in quantum coupling through $\Gamma_{S,D}$, we dispose $\mu_{S,D}$ symmetrically about the equilibrium contact Fermi energy E_F under a source-drain bias V : $\mu_{S,D} = E_F \mp eV/2$. *The contact electrochemical potentials help fix the boundary condition (Dirichlet or Neumann) for Poisson's equation in the contacts, so that the electrostatic potential $\phi(\rho)$ within the device can now develop on its own self-consistently under the applied bias* [23].

The NEGF density matrix equations (Eqs. 7,8) provide the nonequilibrium generalization of Eq. 4. The corre-

spondence is evident by rewriting Eq. 4 as

$$\begin{aligned} n_{\text{eq}}(\vec{r}) &= \rho_{\text{eq}}(\vec{r}, \vec{r}) \\ [\rho_{\text{eq}}] &= \int dE f_0(E - E_F) D(E) \\ &= \int \frac{dE}{2\pi} f_0 G(\Gamma_S + \Gamma_D) G^\dagger \end{aligned} \quad (9)$$

where $[\rho]$ and D are the charge density matrix and the density of states matrix whose diagonal entries give the LDOS and the trace gives the total DOS. The self-consistently converged Green's function G is then used to obtain the current. For coherent transport the NEGF current expression formally resembles that in Landauer theory [18]:

$$\begin{aligned} I &= \frac{2e}{h} \int_{-\infty}^{\infty} dE T(E) [f_S(E) - f_D(E)] \\ T &= \text{Trace}(\Gamma_S G \Gamma_D G^\dagger). \end{aligned} \quad (10)$$

Given an appropriate Hamiltonian H , self-consistent potential ϕ and self-energies Σ , eqns. 5,6,7,8,10 yield a complete set of equations allowing us to obtain the nonequilibrium charge and current densities under bias. Although the equations describe coherent transport, NEGF allows us to handle incoherent processes through additional self-energy matrices determined by the corresponding scattering potentials.

Incoherent processes. Incoherent processes such as hopping or phonon scattering can be included rigorously through a self-energy in the NEGF prescription [24]. A simple, phenomenological way of including this would be to model each scattering center as a floating voltage probe with which the electron equilibrates locally, motivated by Büttiker [18, 25]. Such a probe does not draw any net current, but randomizes the phase of the incoming electrons by reinjecting them into the device. The probe can be parametrized by two quantities, its electrochemical potential μ_p and the self-energy Σ_p . The Green's function expression in Eq. 5 includes the additional self-energy contribution Σ_p , while the transmissions T_{ij} between any of the three contacts is given by $T_{ij} = \text{Trace}(\Gamma_i G \Gamma_j G^\dagger)$, $i, j = S, D, p$.

Besides modifying the transmission, incoherent scattering also affects the local electron density through μ_p , which is fixed by requiring that the net current drawn by the voltage probe is zero. One could model *phase-breaking without energy relaxation*, where the probe Fermi functions $f_p(E)$ are adjusted at *each energy* such that the current $I_p(E)$ drawn by the probe at every individual energy channel is zero. The expression for the net transmission in this case becomes relatively straightforward:

$$T(E) = T_{SD}(E) + \frac{T_{Sp}(E)T_{pD}(E)}{T_{Sp}(E) + T_{pD}(E)} \quad (11)$$

Alternately one could include *energy-relaxation*, adjusting the overall probe electrochemical potential μ_p such that the net probe current $I_p = \int dE I_p(E)$ obtained by integrating the current contributions over various energy channels adds up to zero. One will then need to modify Eq. 10 to include the contributions from the probe to the net source-drain current. The probe self-energy $\Sigma_p(E)$ can be calculated using various models for scattering relaxation. For phonons for example, we use the self-consistent Born approximation [2], whereby the phonon self-energy depends recursively on the electron Green's function. In the limit of low-energy phonons, this amounts to setting $\Sigma_p = \Delta_0 G$, Δ_0 being the coupling between the molecule and the phonon bath. In general, however, the expressions are more complicated [18].

Model Hamiltonians for device and contacts. The above formalism is general, and requires an appropriate Hamiltonian H describing the intrinsic molecular chemistry, an adequate treatment of the geometry and bonding at the contact surfaces described by self-energy matrices $\Sigma_{S,D}$, as well as a suitable self-consistent potential ϕ describing the electrostatics of the device. In the past, we calculated these matrices by modifying a standard quantum chemical software (GAUSSIAN98), self-consistently coupled with a NEGF-based transport formalism [6]. Such a modification allowed us to get I-V characteristics and potential profiles using a density functional (DFT) description of both the molecule and the contacts. While DFT codes allow 'first principles' treatment of electron-electron interactions and quantum correlations with no adjustable parameters, they are tedious and time-consuming. Furthermore incorporating the Poisson boundary conditions typically requires a large chunk of the contacts included along with the molecule within our device [26]. Alternatively, one needs to perform repeated transformations between an orthogonal real space basis where Poisson boundary conditions are readily incorporated, and a non-orthogonal orbital basis suitable for describing the atomic bondings and the molecular chemistry.

In order to bypass the complexities associated with implementing boundary conditions within DFT, we will concentrate here on a much simpler semi-empirical description of the device and contacts, described by an orthogonal basis set $\{\Phi_\mu\}$ of one orbital per atom. Such a basis could, for instance, describe the essential physics of molecular transport through conjugated p_z (π) electron systems, and s electrons for metallic gold wires. In this paper, the scalar on-site and hopping parameters are chosen to match experimental values of the Fermi energy and density of states for gold, as well as the energy eigenvalues and orbital shapes for phenyl dithiol (PDT) calculated using DFT within the local density approximation (LDA) [27] (parameters listed in Table I). The source and drain contacts are modeled as Au(111) surfaces, with the

	On-site (eV)	Hopping (eV)	Hubbard (eV)	Bond-length (Å)
Au-Au	-4.3	8.75	11.13	2.885
C-C	-4.42	2.5	11.13	1.4625
S	-6.32		9.94	
S-C		1.5		1.8
S-Au		1.6		2.885

TABLE I: Semi-empirical parameters used to simulate molecular wires. The S-Au coupling is reduced from 1.6 to 0.8 in the last section to simulate gating of a weakly contacted molecular wire.

wire bonded symmetrically to a surface triangle of gold atoms. The contact self energies $\Sigma_{S,D}$ are obtained rigorously using a real space recursive formalism described elsewhere [6, 11, 28].

Self-consistent potential. The self-consistent potential $\phi(\rho)$ in Eq. 5 can be obtained for a given charge density matrix ρ in a variety of ways. We will ignore the evolution of the exchange-correlation potential under bias (the equilibrium result is incorporated in H), and concentrate only on the Hartree part [29], which depends only on the diagonal elements n of the density matrix. A computationally tedious but accurate way to obtain the Hartree contribution is the direct solution of 3-D Poisson's equation numerically on a real space grid, with appropriate Dirichlet/Neumann boundary conditions at the boundaries (section IV). A faster way, that involves grid points only on the charges and the contacts is the *method of moments* (MOM) [30]. To understand this, one starts by writing the solution to Poisson's equation in matrix form in a suitable basis $\{\Phi\}$, and then partitioning the system into the device ('d') and the contact ('c') sectors:

$$\begin{pmatrix} \phi_d \\ \phi_c \end{pmatrix} = \begin{pmatrix} U_{dd} & U_{dc} \\ U_{cd} & U_{cc} \end{pmatrix} \begin{pmatrix} n_d \\ n_c \end{pmatrix}$$

$$n(\vec{r}) = \rho(\vec{r}, \vec{r}) = \sum_{\mu\nu} \Phi_\mu^*(\vec{r}) \rho_{\mu\nu} \Phi_\nu(\vec{r}), \quad (12)$$

U representing the Hartree term [31]. Eliminating the contact charge density n_c , one gets the device electrostatic potential that is used in Eq. 5 by solving the matrix equation:

$$\begin{aligned} \phi(\rho) \equiv \phi_d &= U_{dc} U_{cc}^{-1} \phi_c + (U_{dd} - U_{dc} U_{cc}^{-1} U_{cd}) n_d \\ &= \phi_L + \phi_P(\rho), \end{aligned} \quad (13)$$

where the Laplace part is the solution to the homogeneous Poisson's equation corresponding to *zero charge in the device* ($n_d = 0$) and specified contact potentials, while the inhomogeneous Poisson part corresponds to the solution for given contact and device charges and with *zero potential on all the contacts* ($\phi_c = 0$). The advantage of MOM is that we need grid points only on the contacts with specified potentials ϕ_c and on the device with specified free charges n_d . The formalism can easily

be extended to include polarization charges in dielectric materials.

In this article, the Coulomb matrices U are obtained using the Pariser-Parr-Pople (PPP) model within the Matago-Nishimoto approximation [32]:

$$U(\vec{r}_i, \vec{r}_j) = \frac{e^2}{|\vec{r}_i - \vec{r}_j| + 1/\gamma_{ij}} \quad (14)$$

where $\gamma_{ij} = 0.5(U_{ii} + U_{jj})/e^2$. The above term interpolates between asymptotic $1/r$ Coulomb repulsion at large distances and on-site Hubbard repulsion U_{ii} at short distances (table I) (Alternate ways of handling the Hubbard term exist; see for e.g. Mc. Lennan *et al.*, [21], Appendix). The effect of image charges on the contact surface atoms is already included in Eq. 13 through the second term in brackets in the expression for $\phi_p(\rho)$. Additional, possibly negligible, image contributions from deeper within the contacts are added in by hand by generating a series of contributions similar to Eq. 14 due to electrostatically infinite planar contacts [33].

The boundary conditions on Poisson's equation are set by the electrochemical potentials $\mu_{S,D}$. One can either use Neumann boundary conditions, requiring overall charge neutrality deep inside the contacts (section IV). Alternatively, one could enforce Dirichlet boundary conditions, setting the electrostatic potentials equal to the electrochemical potentials deep inside the contact (rest of the paper).

Having laid out our general framework and the description of our model Hamiltonians, we will first try to determine how much of the applied bias across a metal-molecule-metal heterostructure drops within the contacts themselves.

III. HOW MUCH VOLTAGE DROPS ACROSS THE MOLECULE?

The transport formalism described in section II applies equally to the device and the contacts. To distinguish between the two, one needs a dilution of modes in going from the contact to the device, such as a drastic change in doping profile (Figs. 2a,b) or a geometrical narrowing of the cross-section (Fig. 2c). A slight deviation from equilibrium inside the contact, integrated over its multiple modes, is then sufficient to drive current through the device, while keeping the contact electrochemical potentials essentially constant. In terms of Eq. 1a, one needs a large conductivity inside the contacts relative to the molecule in order to hold the electrochemical potentials constant inside each contact and drop the applied voltage bias across the molecule itself. For a ballistic device, however, part of the applied voltage drops within the contacts, as we now describe.

To simulate the potential profile under bias across the device as well as the contacts, we will consider an ex-

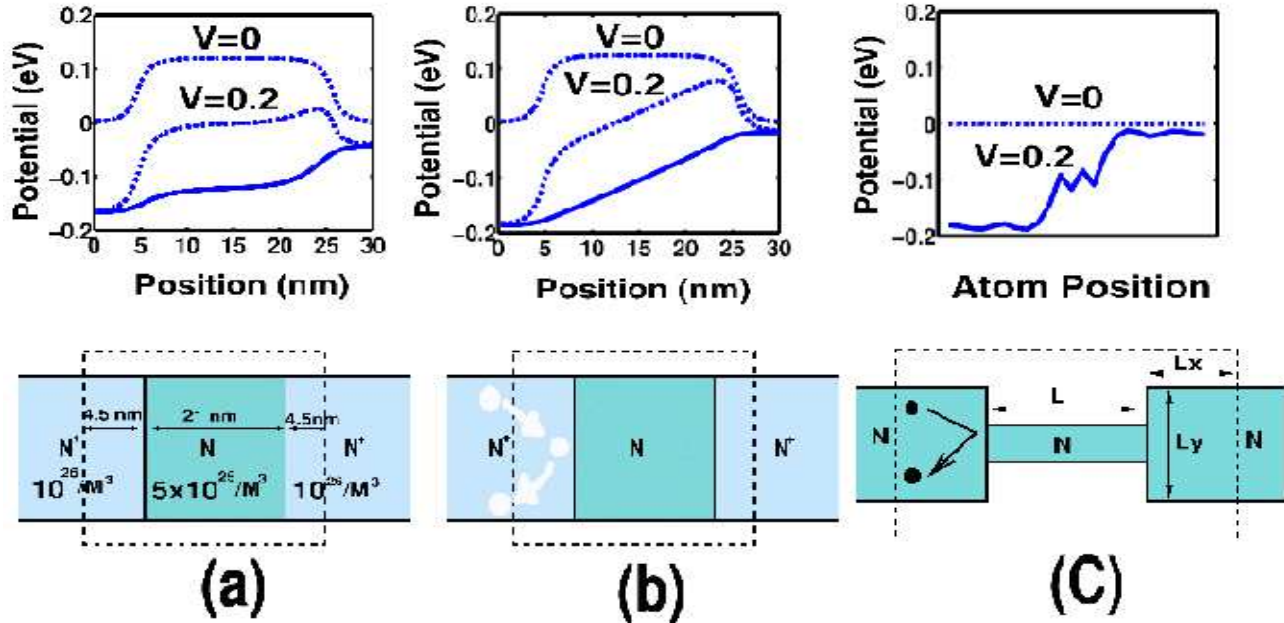


FIG. 2: Electrostatic potential profile in various structures under zero-field boundary conditions (ZFB). Part of the contacts (blue) has been incorporated into the device region within dashed lines. (a) Charge neutrality restrictions due to ZFB in a silicon (n^+nm^+) structure causes the source electrostatic and electrochemical potentials under a 0.2 V bias to separate, thus dropping some of the applied voltage in the contacts. The voltage “loss” can be reduced by (b) increasing scattering or by (c) a geometric dilution (see text), which reduces this mismatch. The structures in (a) and (b) have the same geometry and doping properties, shown in the figure. Structure (c) is simulated by using gold parameters (Table 1). The channel consists of a four atom gold chain, while each contact cluster within the device region consists of a $10(L_x) \times 11(L_y)$ simple cubic gold lattice.

tended device that actually incorporates a large enough part of the contacts to keep it essentially charge neutral. Such an inclusion would automatically take care of image charges for metal contacts or depletion/inversion charges in semiconducting contacts, for example. However, charge neutrality ensures that only a *fraction* of the applied bias appears across the ends of the device, especially if it is ballistic, the rest dropping deeper inside the contacts. It is hard to impose Dirichlet boundary conditions on the electrostatic potential at the two ends without knowing this “lost” fraction a-priori; a better way seems to be to *just fix the electrochemical potentials $\mu_{S,D}$ at the two ends, impose Neumann-type zero-field boundary conditions (ZFB) on the electrostatic potential consistent with Gauss’ law and charge neutrality, and let the potential profile develop on its own self-consistently.*

To illustrate the voltage loss within the contacts described above, we simulate a n-doped device (Fig. 2(a)) consisting of a cluster of silicon atoms of infinite cross-section attached to a n^{++} silicon contact of identical structure and cross-section but with a heavier doping density. Part of the contact has been incorporated into the extended device simulation region (dashed lines) to account for surface charges. The equilibrium ($V = 0$)

potential profile shows a barrier on the device part that reflects the incoming electron waves from the contacts. We determine the potential profile under bias by explicitly solving 1-D Poisson’s equation self-consistently on a real space grid using the Newton-Raphson method [34] with ZFB at the ends. Note also that in the transport equations 8,9,10 one needs to replace each Fermi function $f(E)$ by the corresponding 2-D Fermi function $F_{2D}(E)$ obtained by summing the transverse modes over the two irrelevant dimensions [35],[36]. As is evident from Fig. 2a, applying a 0.2 V source-drain bias lowers the drain electrochemical potential, which in turn lowers the electrostatic potential barrier and leads to current flow. The net self-consistent potential, $\phi(V = 0.2) - \phi(V = 0)$ across the wire is shown in solid line, and exhibits significant screening due to charge rearrangement within the n-doped region. Significantly, lowering the drain electrochemical potential also lowers the source electrostatic potential, implying that *only a fraction of the applied 0.2 V bias actually appears across the simulated region.* To understand this, we recall that in a ballistic device the current carrying electrons can be grouped into $+k$ and $-k$ states that originate in the drain and source contacts respectively [18]. A bias changes the occupancies

of these states, so that a current flows due to their imbalance. Inside the source contact too, a bias produces a similar imbalance between $+k$ and $-k$ states, with the result that part of the electron states inside the source end up being depopulated by the drain electrode. The depopulation forces part of the applied bias to drop inside the source contact in order to keep it charge neutral [37]. Consequently, only a fraction of the applied bias occurs across the two ends.

The depopulation of the source contact is particularly noticeable for ballistic transport, where the drain end can effectively empty out the source end and lower its electrostatic potential significantly. This observation seems to be in keeping with Landauer's idea that only a fraction R (R : device reflection coefficient) of the applied bias actually appears across the active device, which in conjunction with a current proportional to the transmission T gives the celebrated Landauer conductance for a single-mode structure minus the interfaces, $G = (2e^2/h)(T/R)$ [38]. It seems evident therefore that the way to eliminate the voltage loss for a ballistic device is to increase the average scattering ($R \rightarrow 1$), which would in effect isolate the source and drain and prevent the latter from depopulating the former. This could be achieved by increasing the doping density in the n^{++} region of Fig. 2(a), by increasing scattering throughout the device (Fig. 2(b)), or by enforcing a geometric dilution with a flared-out contact geometry (Fig. 2(c)). In (b) we use Büttiker probes to simulate scattering, while in (c) we solve the 2-D Poisson equation to take care of the varying transverse cross-sectional geometry, using the relevant F_{1D} function obtained by summing the Fermi-Dirac function over the single irrelevant dimension. As we see in both cases, a larger fraction of the applied bias appears across the ends with a smaller voltage loss in the contacts, as evidenced by the closer agreement between the electrostatic potential values at $V = 0$ and $V = 0.2$ V deep within the source [39]. Scattering in the contacts can thus have a significant influence on the device conductivity, tending to make it robust with respect to spatial variations in the interfacial geometry [40].

In the simulations we present hereafter, we will explicitly incorporate a built-up, atomistic part of the contacts along with the molecule within our device, enforcing thereby a geometric dilution. Accordingly, we will assume that most of the applied bias appears across the ends, with minimum voltage loss in the contacts [41]. This assumption will allow us to switch to Dirichlet boundary conditions imposed on the potential profile, which ends up being computationally easier to handle. Since the contact potentials are assumed specified hereafter, we will use the MOM instead of explicitly solving Poisson's equation on a real space grid.

IV. POTENTIAL SCREENING INSIDE A WIRE: THICK VS. THIN

We will now concentrate on the potential profile inside the wire, and discuss how its overall shape is determined by broad, macroscopic geometrical features such as the wire thickness and screening length. We will see that screening is ineffective in a wire that is thinner than its Debye length. Later on, we will talk about finer details, determined by the internal molecular structure of the wire itself.

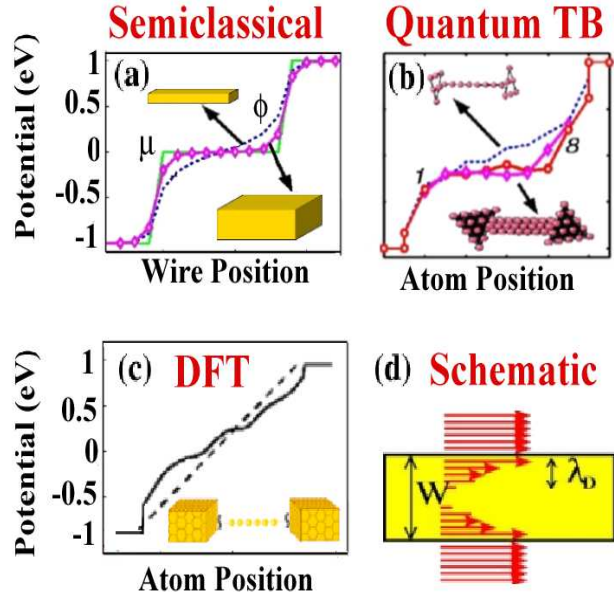


FIG. 3: Electrostatic potential profile under two volts applied bias for ballistic thin and thick wires (devices simulated shown as insets) using (a) semiclassical modeling with a continuum structure; (b) quantum tight-binding modeling with an atomistic structure, and (c) fully ab-initio DFT modeling (adapted with permission from [6]). Symbols represent the positions of the atoms along the device. The electrostatic potential drop along the wire decreases from thin to thick wire due to increased feasibility of increased transverse screening when the wire thickness W exceeds the Debye length λ_D , for which the field lines are shown schematically in (d). In the quantum calculations (b) and (c), the potential profile exhibits Friedel oscillations superposed on the long-wavelength Debye screening. Self-consistent charging under bias leads to a voltage asymmetry (see explanation in text as well as caption of Fig. 4), although the I-V remains symmetric with respect to bias direction.

Fig. 3(a) shows the potential profiles for a wire with a 2 volt applied bias, using a semiclassical, continuum approximation (Eq. 1). The wire is 9 atoms long, while the contact block is 8 atoms long (only 3 atoms plotted) and 5×5 atoms in cross-section. The solid line shows the average electrochemical potential along the wire, which is spatially unvarying along the ballistic wire and drops

only at the contact interfaces. Using this electrochemical potential μ as a driving term in Eq. 1b gives the electrostatic potential profile ϕ . The Debye lengths of the contact and the wire regions are each assumed to be half the interatomic separation. For a thick slab representing the wire (3x3 atoms in cross-section, geometry shown lower right), the potential profile (diamonds) is well-screened by charge rearrangement in the material of the wire described by the Poisson part $\phi_p(\rho)$. As we progressively thin the wire, however, we reach a point where the thickness of the wire is no longer much smaller than the Debye length (1x1 atom in cross-section, inset top left), at which point transverse charge screening become ineffective. This causes the field lines to penetrate in the transverse direction, generating a large ramp-like electrostatic potential profile along the wire (dashed line), essentially exhibiting just the Laplace solution ϕ_L . A continuum analysis by Nitzan *et al.* leads to a similar conclusion, showing the dependence of the slope of the potential on the wire length, thickness and screening parameter [16].

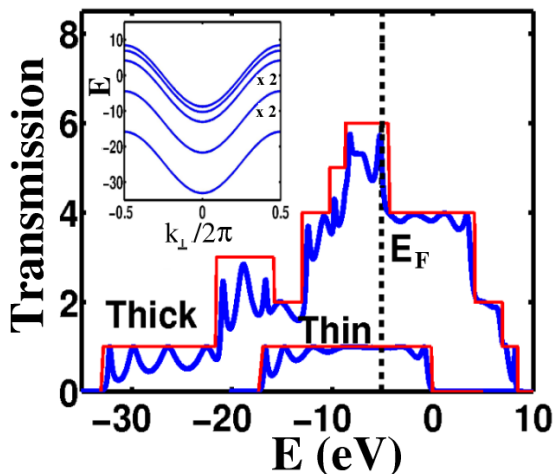


FIG. 4: Equilibrium transmission of thin and thick wires both show fine structure associated with Fabry-Perot end effects (blue solid line) superposed on the overall structure associated with transverse modes (mode transmissions in red). The multiplicity of channels for a thick wire (subband structure shown in inset) arising due to quantization of the transverse (k_{\perp}) quasimomentum leads to the overall structure in its transmission (red). Under a small positive source bias, the drain electrochemical potential adds less negative charge to the thick wire than the source depletes, owing to the proximity of the Fermi energy with a transmission mode bandedge that lies just above it in energy. The net positive charge floats down the molecular levels relative to E_F , giving rise to the asymmetry in the potential profiles in Fig. 3b.

In Fig. 3(b), we arrive at the same conclusions, albeit from a more rigorous atomistic model Hamiltonian, including self-consistent charging effects and the detailed

bonding geometry at the Au(111) contacts, and employing the full machinery of the quantum kinetic NEGF transport formalism (Eqs. 5-13,14). The same two cases are studied as before, with a thin wire constructed out of a chain of eight gold atoms connected to a triangle of FCC Au(111) contact surface atoms (top left), and a thicker version generated by enclosing the central wire in a sheath of six identical gold wires around it (bottom right). The wires have quantum mechanical couplings in the transverse direction as well, allowing charge flow in that direction. Contacting the wires to the 3-D gold leads leads to a dimensionality mismatch and an associated work-function mismatch, transferring about 0.8 electrons at equilibrium to the thin wire and 2 electrons to the thick wire (the charging energy per electron U_0 is about 2-3 eV for the thin and 1.1 eV for the thick wire, so the work function mismatch leads to a band adjustment of about 2 eV for both thin and thick wires at equilibrium). The electrostatic potential profile along the central wire progressively changes from flat (diamonds) to ramp (dashed line) as the surrounding wires are removed [41]. A DFT version with a six atom gold wire (Fig. 3c) [6] shows a similar profile. The screening along the transverse direction (Fig. 3d) is feasible only if the wire thickness W exceeds the Debye length λ_D . The oscillations in the potential profile arise due to coherent Friedel oscillations (discussed later). A part of the potential drops across the end triangle of contact atoms (symbols 1 and 8 referring to the end wire atoms in b). Interestingly, even the surface potential along the thick wire (circles) shows screening although it is exposed on least one side. We believe the other wires screen the field over a large enough angle of the cross section that the field penetrating from the exposed part is minimal.

The potential profile for the thin wire is spatially symmetric, but that of the thick wire shows a significant amount of asymmetry. This asymmetry arises from self-consistent charging effects in the wire associated with its quantum capacitance. While the transmission of the thin wire is effectively structureless and approximately unity over a band (except for Fabry-Perot type resonances near the band-edges), the transmission of the thicker wire has considerable structure owing to the availability of various transverse modes that kick in and out at various energies. Fig.4 shows the zero bias, non self-consistent transmissions for a thin and a thick wire. The transmissions show a rapid oscillatory structure (blue solid lines) due to Fabry-Perot effects from the end superposed on a broader structure that arises from the transverse modes of the wires (red solid lines). For the thin 1-D wire, the transmission is unity between the band edges. For the thick wire, however, one can support multiple transverse modes associated with the seven wires (subband structure shown in inset; there are seven subbands, of which some are doubly degenerate, denoted by ‘x 2’). At 2 V bias the existence of an edge in the transmission mode

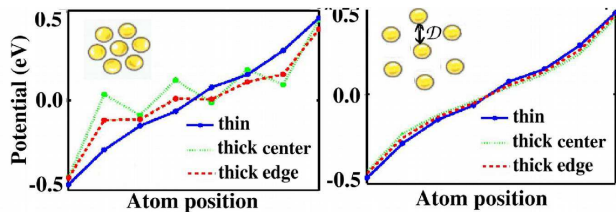


FIG. 5: Decrease in screening as a thick wire is pulled apart (same geometry and applied bias as in Fig. 3b, with only the part between atoms 1 and 8 shown here). For a closely packed coaxial wire, the potential profile of the central wire was screened (Fig. 3b, diamonds) compared to the thin wire (blue dotted line above, and blue dashed line in Fig. 3b). The screening is reduced drastically on pulling the wires just a little bit (left), since it eliminates the quantum couplings among the wires and prohibits rearrangement of screening charges in the transverse direction. The electrostatic coupling between wires is longer ranged, and is eliminated once the inter-wire separation \mathcal{D} becomes comparable to the maximum distance between a charge and the nearest source/drain ground plane, i.e., half the wire length. The potential profile (right) of each wire now resembles that of an individual thin wire.

spectrum above E_F causes the source electrochemical potential to add less charge to the wire than the drain removes, so about 0.08 electrons are removed from the thick wire. The average single-electron charging energy of the thick wire, ~ 1.1 eV/electron causes a shift in average potential profile associated with the charge depletion by ~ 0.09 eV. The shift gets localized on only the central 5 atoms or so where charge depletion is most, so the local electrostatic potentials at those points get lowered by about $0.14 - 0.2$ V relative to E_F , as in Fig. 3b, making the overall electrostatic potential profile asymmetric. Such an asymmetry due to charging arises whenever the transmission spectrum has significant structure, as for a multimoded wire or a molecular conductor like PDT with distinct asymmetric highest occupied (HOMO) and lowest unoccupied (LUMO) levels. However, this charging effect is not readily observed experimentally, because it does not affect the I-V directly. Although charging makes the potential profile asymmetric, the I-V is symmetric with drain bias because the sense of the asymmetry reverses perfectly on reversing bias, so that the I-V does not show any sign of rectification [42].

It is interesting to see how the screening effects get diluted as the thick wire is progressively taken apart into its constituents. Fig. 5 (left) shows the hexagonal sheath of wires (cross-section shown in the inset) undergoing such a decimation process. First we lose the quantum couplings between adjacent wires, valid at a small increase in separation \mathcal{D} between them. This process in essence localizes the charges to the individual wires, disallowing any transverse charge rearrangement and making transverse screening quite inefficient. The corresponding electrostatic potential profile starts to look unscreened, like

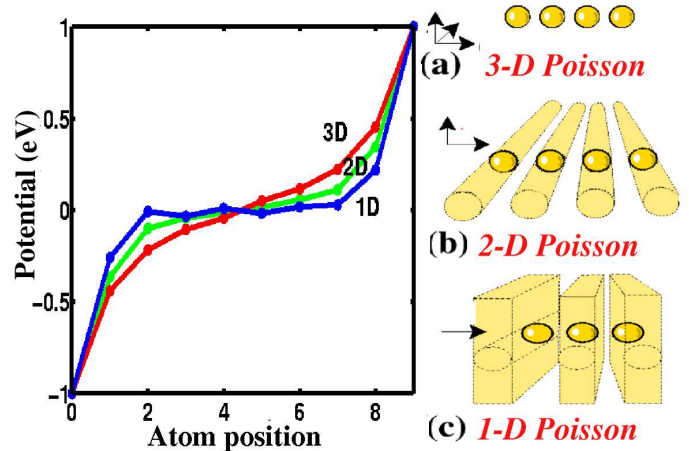


FIG. 6: Dependence of the electrostatic potential on the dimensionality of the electric field: (a) single atomic wire simulated with 3-D Poisson's equation; (b) 2-D distribution of charges and fields, with no transverse variations, corresponding to a single SAM layer. Each wire atomic charge is smeared out into a line along the layer direction; (c) variation allowed only in 1-D, corresponding to a close-packed SAM or a molecular solid, with the charge on each atom smeared out into a 2-D sheet along the SAM cross-section. A SAM screens fields in the transverse direction better, hence the trend in the potential profile with reducing dimensionality of the field lines.

a ramp, being affected only by limited transverse flow of charge within each wire, around the individual atomic cores. The coupling at this stage is electrostatic, given by the inter-wire capacitances, which decrease linearly with \mathcal{D} . Finally, when $\mathcal{D} \approx L/2$, where L is the wire length, the capacitive couplings with the source and drain electrodes dominate over the inter-wire capacitances, and the wire charges image on the nearer electrodes instead of on neighboring wires. At this stage, the assembly behaves in essence like unscreened wires, with each of their individual potential profiles (Fig. 5, right) resembling the ramp-like profile of an isolated wire (blue dotted line).

In this section, we saw that *screening is ineffective for a wire that is thinner than its Debye length*. This is because of the feasibility of unscreened fields penetrating along the transverse direction (Fig. 3(d)) that can lead effectively to a poor overall screening. Transverse screening can be improved by reducing the cross-section of the contacts. This eliminates field lines away from the contacts, generating a Laplace solution that is itself flat in between the two contacts. In our calculations, however, specifying the potential boundary conditions on the thin contact cross-sections alone is not sufficient to allow the method of moments to converge readily to a solution, due to incomplete specification of boundary conditions. Convergence requires fixing the potential at a large distance, as if on imaginary gate electrodes. Similar conclusions have been obtained for ideal 1-D wires [43]. It has been shown, for instance, that long-ranged longitudinal

screening is ineffective in conductors such as metallic nanotubes where the charge transport is in 1-D (along the axial direction of the nanotube surface). Thus doping the nanotube at an interface leads to an asymptotically nonvanishing surface charge along the nanotube [17].

V. POTENTIAL SCREENING BY THE ENVIRONMENT: SINGLE MOLECULE VS. MONOLAYER

We have seen that the efficiency of voltage screening depends on the availability of adequate wire thickness to enable sufficient charge reorganization in the transverse direction. Thus for thin wires in isolation, such as in a break-junction experiment, screening is incomplete and the potential profile is essentially given by the Laplace part ϕ_L . In contrast, embedding the wire inside a self-assembled monolayer (SAM) allows sufficient charge rearrangement among wires, so that the transverse fields can be efficiently screened out by neighboring wires. We investigated transverse screening by neighboring wires by modeling a SAM that is very densely packed. For wire separation much smaller than the wire length (half the length to be precise, as we saw in the previous section), one could ignore charge and potential variations in the transverse direction. This process amounts to replacing the 3-D Poisson equation with a 2-D version that smears each gold atom into a transverse wire generating a mat of gold atoms, or a 1-D version smearing each gold atom into a sheet generating a block or SAM of gold atoms (Fig. 6). Instead of actually solving Poisson's equation in reduced dimensions for each case, we replace the PPP 3-D Green's function in Eq. 14 with a 2-D version $U(\vec{r}_i, \vec{r}_j) \propto \ln |\vec{r}_i - \vec{r}_j|$ and with the 1-D version $U(x_i, x_j) \propto \min(|x_i - x_j|, L - |x_i - x_j|)$. For transport, we assume that the wires are separated and do not have strong transverse couplings, so that one does not obtain a transverse band of energies. Charge cannot flow easily in the transverse directions by hopping from wire to wire, and one gets essentially several copies of the same wire along the transverse directions. This means that instead of using F_{1D} and F_{2D} functions along with the 2-D and 1-D Poisson equations like we did in section IV, we use $f(E)N_l$ and $f(E)N_A$, where N_l and N_A respectively denote the number of wires per unit length and the number per unit area.

The resulting self-consistent potentials are shown in Fig. 6. The inter-wire separations for the 2-D and 3-D cases are assumed to be equal to the separation between gold atoms (2.885 Å) within the wire. From the figure, we see that as the Poisson equation is shifted to lower dimensions corresponding to the inclusion of more and more neighboring wires, the potential profile gets progressively flatter due to enhanced screening efficiency of the transverse modes, so that the 1-D Poisson profile ap-

pears well-screened [5].

VI. INTRAMOLECULAR POTENTIAL VARIATIONS

The previous sections dealt with the broad shape of the potential profile across a molecular conductor. As was evident from Fig. 3, the qualitative features of the potential profile can basically be understood in terms of simple semiclassical continuum pictures, except for Friedel oscillations and issues relating to the molecular density of states and single-electron charging. The question may arise at this stage as to whether the sophisticated machinery of quantum transport and NEGF, or the quantum Hamiltonian and atomicity of the device are important at all and whether they could have observable consequences beyond what is predicted from a continuum description. The answer is that it could matter, specifically for processes that involve the chemistry of the molecule. Specifically, we will discuss two such examples: (i) potential barriers in PDT, and (ii) features related to the alignment of levels localized on different parts of the molecule, such as those generating a diode-like I-V or a negative differential resistance (NDR).

Fig. 7 shows the electronic charge distribution on PDT at equilibrium and under a 2 volt bias. Fig. 8 shows the corresponding electrostatic potential profile, including gold clusters at the end. The result, obtained from a semiempirical calculation, compares well with DFT calculations performed elsewhere [6]. The largest voltage drop occurs between the end sulphur and gold atoms, with the sulphur atoms acting as a barrier (Fig. 7 and Fig. 8), and minimal voltage drop within the gold cluster itself. The sulphur barrier is formed because of the ionic Au-S bonds, which involve transfer of electrons from the gold leads onto the electronegative sulphur atoms. Although it is hard to measure such an atomic barrier experimentally, it is instructive to note that the barriers on sulphur do control the magnitude of the current to some extent, although the thinness of the barrier (few Angstroms) probably allows substantial electron tunneling through it. Furthermore, the barrier regulates the flow of current, causing charge to pile up there under bias forming a residual resistivity dipole, as the current rearranges to go around the benzene ring (Fig. 7).

Atomistic barriers and defects can regulate the directionality and magnitude of current flow patterns within the molecule. In addition, coherent transport of electrons leads to Friedel oscillations in the potential profile around the defects and interfaces (Fig.3b; also see [6, 44]). This is a purely quantum mechanical phenomenon arising from the sharpness of the Fermi surface at low temperature. The Friedel oscillations are superposed on the long-wavelength Debye screening described earlier. The coherent oscillations can be elim-

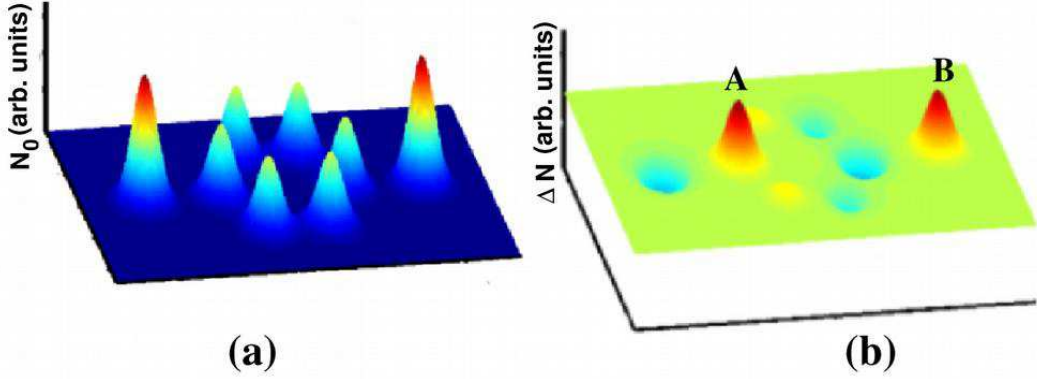


FIG. 7: (a) Electronic charge distribution in PDT at equilibrium, smoothed artificially using a single Gaussian function for clarity. There is a distinct barrier on the sulphur atoms due to electron transfer from gold electrodes. (b) Change in electron distribution under bias shows an overall electron flow to the right. Charge piles up at points A and B generating two residual resistivity dipoles, as current needs to flow around the benzene ring.

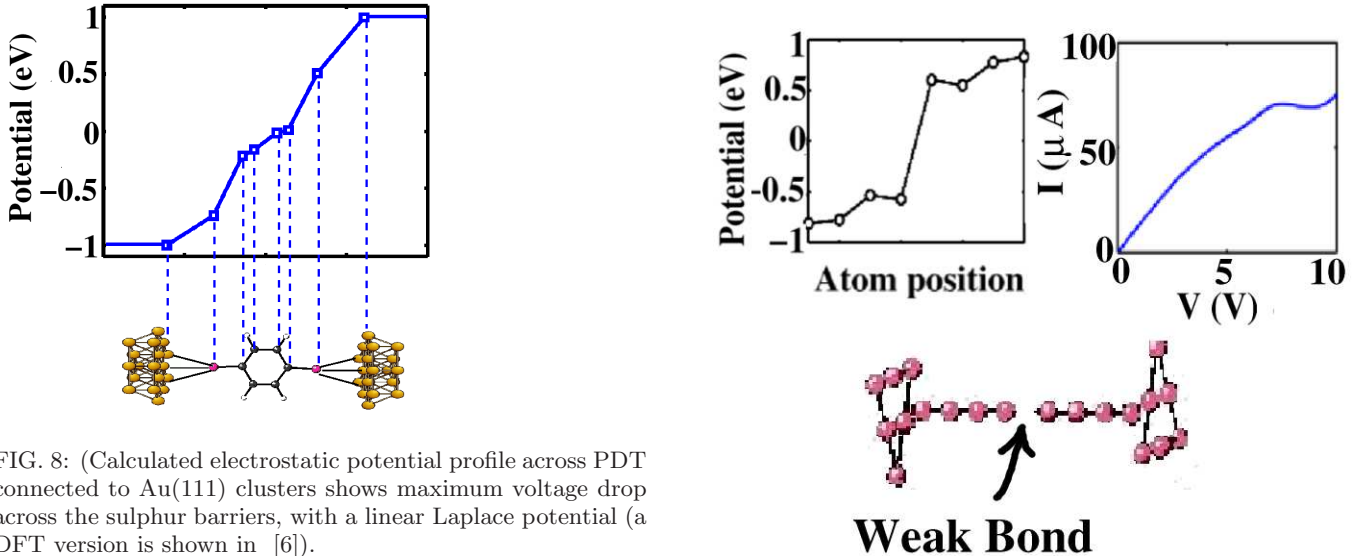


FIG. 8: (Calculated electrostatic potential profile across PDT connected to Au(111) clusters shows maximum voltage drop across the sulphur barriers, with a linear Laplace potential (a DFT version is shown in [6]).

inated by incorporating incoherent scattering into the molecule through Büttiker probes ([6, 44]).

The intramolecular electrostatic potential determines the local energy levels and the local density of states (LDOS), so that any substantial potential variation could bring various parts of the molecule in and out of resonance. Such resonances can lead to observable consequences, such as generating an asymmetric, diode-like I-V by bringing the donor and acceptor levels at two ends of a molecule in and out of resonance (Aviram-Ratner mechanism) [10]. An analogous process is shown in Fig. 9, where an artificially weakened bond in a QPC leads to maximum potential drop across it, separating the wire into two parts that separately equilibrate with the gold leads they are in contact with. The LDOS of the two parts slide past each other due to $\phi_L(\vec{r})$, bringing transmission peaks on both sides in and out of resonance. Such

FIG. 9: Most of the applied bias drops across a weakened bond in a QPC (top left), effectively separating the two sides which individually equilibrate with the corresponding metal contacts. The QPC I-V shows a weak NDR (top right) due to voltage-induced alignment and misalignment of the LDOS on both sides of the defect (a DFT version is shown in [11]).

a resonance leads to a weak NDR [33] (a DFT-based version was demonstrated earlier, in [44]).

VII. INFLUENCE OF REMOTE CONTACTS: GATE MODULATION

We have seen that the conductance of a molecule can be influenced simply by the Laplace part of the electrostatic potential, which depends on the geometry and

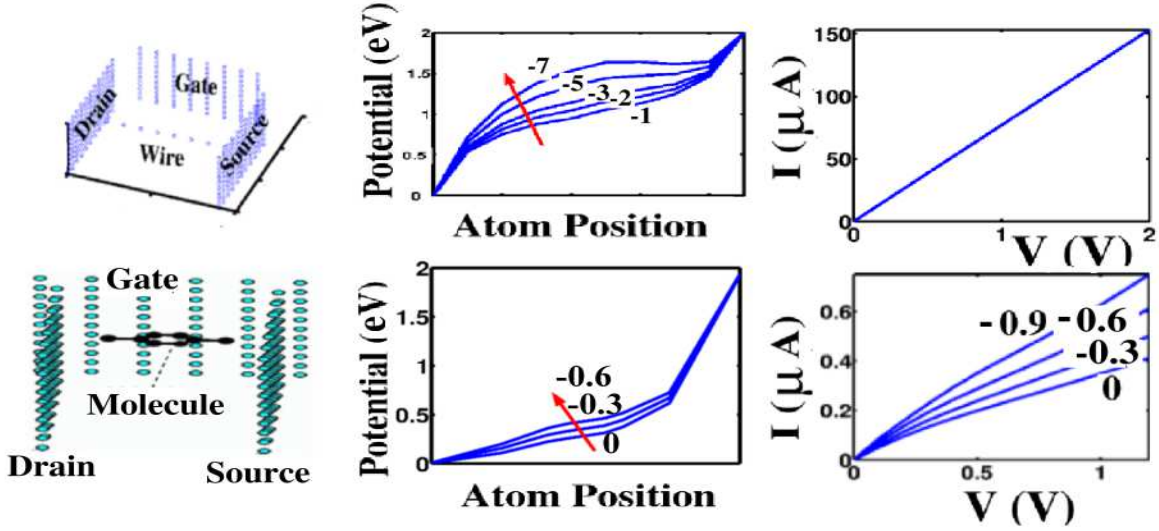


FIG. 10: Influence of a gate on the molecular I-V for (a) a gold wire and (b) a PDT molecule placed near the gate (gate is placed 1.5 nm away from the gold wire and 2.9 Å from PDT). The gate controls the device potential and shifts the molecular levels relative to the contact electrochemical potentials. The current is unaffected for a gold wire due to its relatively featureless density of states that make it insensitive to level shifting. For PDT, the current tends to saturate when the drain electrochemical potential ventures into the HOMO-LUMO gap. The gate control, however, is quite poor due to the poor aspect-ratio in the problem, as well as metal-induced gap states (MIGS) from the gold contacts. Furthermore, the system is expected to have considerable gate leakage due to the thinness of the gate insulator (vacuum in this treatment), making the molecule a poor transistor. The gating can be improved in principle by using longer molecules with doped silicon contacts as source and drain, and high-k gate insulators to eliminate gate leakage currents.

shape of the source and drain contacts. In addition, the potential profile in a conductor can be substantially influenced by the presence of a third (gate) electrode (Fig. 10, top left). Image charges on the gate electrode de-emphasize the Poisson solution, so that the gate-induced molecular potential is essentially a Laplace contribution ϕ_L . A negative gate bias raises the molecular energy levels by increasing the average electrostatic potential ϕ_L (Fig. 10, top center) relative to the contact Fermi energy. For a molecule with constant DOS such as a thin gold wire, this shift does not affect the I-V, which remains ohmic with a quantized conductance $G_0 = 2e^2/h \approx 77\mu\text{S}$ for varying gate voltage values (Fig. 10, top right). The relative insensitivity of the conductance quantization to the contact geometry has been discussed at length in several papers [45]. However, for a transistor involving a molecule such as PDT (Fig. 10, bottom left) having a DOS with a lot of structure associated with broadened HOMO and LUMO levels, the overall potential shift affects the zero-bias conductance. For PDT, the conductance increases with increasing negative gate voltage because the molecule is essentially p-type (closest conducting level to E_F is HOMO-based). In addition, the potential profile is skewed towards the source-end (Fig. 10, bottom center), which has a common ground with the gate electrode. Good gate control in a “well-tempered” metal oxide semiconductor field effect transistor (MOSFET) makes the Laplace potential insensitive to source-drain bias and sets it by the source-gate bias instead (as in Fig. 10) [46]. The asymmetric potential profile effectively

tends to pin the channel potential to the source electrochemical potential, so that only the electrochemical potential of the drain electrode varies under source-drain bias. For negative drain bias, the drain electrochemical potential μ_D enters the molecular HOMO-LUMO gap (HLG), leading to an I-V characteristic with decreasing slope due to a decreasing DOS in the gap (Fig. 10, bottom right). Different gate voltages yield different zero-bias values E_F for the drain electrochemical potential μ_D relative to the levels. This gives a gate-voltage dependence of the saturation current, leading to MOSFET-like I-V characteristics with gate modulation [27, 47].

While the above gate control mechanism describes the principle of operation of an ideal ballistic silicon MOSFET [46], the quantitative conclusions (saturation, gate modulation) are usually severely compromised when the MOSFET is scaled to molecular dimensions. Electrostatic gate control requires the gate electrode to be substantially closer to the molecule than the source-drain electrodes, while good saturation in the IVs (large impedances) require a vanishing DOS in the HLG. For long molecules [15] one can have a modest oxide thicknesses that still yields appreciable gate control. However, for small molecules ~ 10 Å, the oxide thickness cannot be scaled down enough without causing dielectric breakdown, leading to poor electrostatic gate control [27]. Furthermore, the current saturation is poor (Fig. 10) due to a non-negligible gap DOS arising from the broad HOMO tails generated by MIGS from the gold contacts. Improving the gate control and the impedance require the uti-

lization of high-k gate dielectrics and degenerately doped semiconducting contacts. Alternately, one could envision transistor action based on non-electrostatic principles, such as by gating the molecular conformations, for example [50].

The gate control can be enhanced by wrapping the molecule with cylindrical gates surrounding the wire. Such a scheme is employed in silicon transistors to produce dual-gate MOSFETS [51], FINFETs [52] or structures with wrap-around gates [53]. We have modeled the effect of multiple gates by placing two, three and four rectangular gate electrodes symmetrically around the wire. Increasing the number of gate electrodes increases the potential barrier, along with an overall increase in the average potential. This leads to superior gate control. The practicality of this scheme, however, depends on the capacity to have multiple gates closely spaced around the molecular wire and insulated from it.

IX. CONCLUSIONS

The electrostatic potential profile across a conductor controls the distribution and magnitude of current across it. While broader features such as the overall conductivity and screening lengths determine the shape of the I-V curves in many cases, atomistic features involving level resonances can influence these I-Vs in a nontrivial way, necessitating a proper atomistic, quantum kinetic treatment of charge transport in molecular devices. We have performed such a treatment within a coupled Poisson-NEGF formalism, while simplifying the molecular chemistry to essentially one orbital per atom for computational simplicity and ease of illustration (a more sophisticated DFT version for some of these profiles has been demonstrated elsewhere). We have seen that the Poisson part of the electrostatic potential profile depends on the strength of transverse and longitudinal screening, and can yield nontrivial charging effects. A gate electrode generates image charges that deemphasize the role of the Poisson part, while modulating the Laplace solution suitably to significantly alter the device I-V characteristic and yield saturating currents. However, feasibility of electrostatic gate control depends on the channel length to oxide thickness aspect-ratio in the problem, and may need to be supplanted by alternate physical principles, such as employing conformational degrees of freedom for example.

We would like to thank P. Damle, J. Guo, T. Rakhshid, R. Venugopal, A. Nitzan, P. Solomon and F. Zahid for useful discussions. This work has been supported by ARO-DURINT, Award# 527826-02, and NSF, Award# 0085516-EEC.

-
- * Electronic address: liangg@ecn.purdue.edu
 † Electronic address: ghosha@ecn.purdue.edu
- [1] M. A. Reed, C. Zhou, C. J. Muller, T. P. Burgin, and J. M. Tour, *Science* **278**, 252 (1997).
 - [2] W. D. Tian, S. Datta, S. H. Hong, R. Reifengerger, J. I. Henderson, C. P. Kubiak, *J. Chem. Phys.* **109**, 2874 (1998).
 - [3] J. Reichert, R. Ochs, D. Beckmann, H. B. Weber, M. Mayor and H. von Lohneysen, *Phys. Rev. Lett.* **88**, 176804 (2002).
 - [4] R.M. Metzger, B. Chen, U. Hopfner, M. V. Lakshmikantham, D. Vuillaume, T. Kawai, X. L. Wu, H. Tachibana, T.V. Hughes, H. Sakurai, J. W. Baldwin, C. Hosch, M. P. Cava, L. Brehmer, and G. J. Ashwell, *J. Am. Chem. Soc.* **119**, 10455 (1997); J. Chen, M. A. Reed, A. M. Rawlett, and J. M. Tour, *et al.*, *Science* **286**, 1550 (1999); A. Dhirani, P.-H. Lin, P. Guyot-Sionnest, R. W. Zehner and L. R. Sita, *J. Chem. Phys.* **106**, 5249 (1997); X. D. Cui, A. Primak, X. Zarate, J. Tomfohr, O. F. Sankey, A. L. Moore, T. A. Moore, D. Gust, G. Harris and S. M. Lindsay, *Science* **294**, 571 (2001); D. Porath, A. Bezryadin, S. de Vries and C. Dekker, *Nature* **403**, 635 (2000).
 - [5] V. Mujica, A. Roitberg and M. Ratner, *J. Chem. Phys.* **112**, 6834 (2000).
 - [6] P. S. Damle, A. W. Ghosh and S. Datta, *Phys. Rev. B* **64**, 201403 (R) (2001).
 - [7] N. D. Lang and P. Avouris, *Phys. Rev. Lett.* **84**, 358 (2000); N. D. Lang and P. Avouris, *Nano Lett.* **3**, 737 (2003).
 - [8] M. Brandbyge, J.-L. Mozos, P. Ordejon, J. Taylor and K. Stokbro, *Phys. Rev. B* **65**, 165401 (2002).
 - [9] E. Louis, J. A. Vergés, J. J. Palacios, A. J. Pérez-Jiménez, and E. SanFabián, *Phys. Rev. B* **67**, 155321 (2003).
 - [10] A. Aviram and M. A. Ratner, *Chem. Phys. Lett.* **29**, 274 (1974).
 - [11] P. S. Damle, A. W. Ghosh and S. Datta, *Chem. Phys.* **281**, 171 (2002).
 - [12] S. Datta, W. Tian, S. Hong, R. Reifengerger, J. I. Henderson and C. P. Kubiak, *Phys. Rev. Lett.* **79**, 2530 (1997).
 - [13] A. W. Ghosh and S. Datta, *J. Comp. El.* **1**, 515 (2002).
 - [14] A. Bachtold, M. S. Fuhrer, S. Plyasunov, M. Forero, E. H. Anderson, A. Zettl and P. L. McEuen, *Phys. Rev. Lett.* **84**, 6082 (2000).
 - [15] K. Sheshadri and C. Frisbie, *Appl. Phys. Lett.* **78**, 993 (2001).
 - [16] S. Pleutin, H. Grabert, G-L. Ingold and A. Nitzan, *J. Chem. Phys.* **118**, 3756 (2003); A. Nitzan, M. Galperin, G-L. Ingold and H. Grabert, *J. Chem. Phys.* **117**, 10837 (2002).
 - [17] F. Léonard and J. Tersoff, *Phys. Rev. Lett.* **83**, 5174 (1999); A. A. Odintsov, *Phys. Rev. Lett.* **85**, 150 (2000).
 - [18] S. Datta, "Electronic Transport in Mesoscopic Systems", Cambridge University Press (1995).
 - [19] For a 3-D noninteracting electron gas this gives $\lambda_D = \sqrt{2\epsilon E_F/3n_{eq}e^2}$, where E_F is the Fermi energy and n_{eq} is the equilibrium electron density. For a classical electron gas at temperature T one simply replaces $E_F \rightarrow 3/2k_B T$.
 - [20] M. Krčmar, W. M. Saslow and A. Zangwill, *J. Appl. Phys.* **93**, 3495 (2003).
 - [21] M. J. McLennan, Y. Lee and S. Datta, *Phys. Rev. B* **43**,

- 13846 (1991).
- [22] A classic example is a p-n junction at equilibrium, where the electrochemical potential is constant while the electrostatic potential varies over a depletion width, generating a built-in electric field across the junction. Note that for a semiconductor, the conductivity σ depends on the potential ϕ through band-bending.
- [23] The choice of values for $\mu_{S,D}$ is gauge-invariant. If we add a constant to the contact electrochemical potentials, the extra charge on the contacts would cause the contact levels to float up, so that the added constant will get incorporated into the Laplace part ϕ_L of the electrostatic potential.
- [24] R. Lake, G. Klimeck, R. C. Bowen and D. Jovanovic, *J. App. Phys.* **81**, 7845 (1997).
- [25] M. Büttiker, *Phys. Rev. B* **33**, 3020 (1986).
- [26] P. Damle, Ph. D. Thesis, Purdue University, 2003.
- [27] P. Damle, T. Rakshit, M. Paulsson and S. Datta, *IEEE Trans. Nanotech.* **1**, 145 (2002).
- [28] M. Samanta, Master's thesis, Purdue University, 1999.
- [29] The evolution of the exchange-correlation part can be taken into account if instead of just iterating the Poisson's equation, one iterates a proper DFT Hamiltonian with appropriate boundary conditions, self-consistently coupled with NEGF. Such a scheme has been used in [6], with an improved treatment of the boundary conditions for the Hartree part described in [26]. Here, we concentrate on just the evolution of the Hartree part under bias, in keeping with the main focus of our paper.
- [30] S. Ramo, J. R. Whinnery and T. Van Duzer, "Field and Wave in communication electronics", John Wiley and Sons, Inc. (1993).
- [31] The matrix product in Eq. 12 translates into an integral representation of Poisson's solution, when expanded in terms of the matrix indices.
- [32] J. N. Murrell and A. J. Hager, *Semi-Empirical SCF MO Theory of Molecules* (Wiley, London, 1972).
- [33] M. Paulsson and S. Stafström, *Phys. Rev. B* **64**, 035416 (2001).
- [34] D. J. Rose and R. E. Bank, *Numerische Mathematik* pp. 279 (1981).
- [35] P. S. Damle, A. W. Ghosh and S. Datta in "Molecular Nanoelectronics", American Scientific Publishers (2003).
- [36] The dimensional subscript for the F functions describes the trivially summed dimensions, and when combined with the dimension of the explicitly solved Poisson's equation, should add up to three.
- [37] S. Datta, *Superlat. Microstruct.* **28**, 253 (2000).
- [38] R. Landauer, *Zeitschrift für Phys. B* **68**, 217 (1987).
- [39] Oscillations in (c) arise due to imperfect bondings with simple cubic contacts, employed for simplicity in this calculation.
- [40] R. Venugopal, *private communications*.
- [41] As explained in section III, including built-up regions of the contact within the device leads automatically to a geometric dilution that reduces the amount of the applied voltage lost within the contacts. This is confirmed by increasing the size of the contact region, which does not affect the voltage dropped across the wire. The potential profile inside the contact flattens out and reaches the applied bias within a couple of layers from the wire surface.
- [42] V. Mujica, M. A. Ratner and A. Nitzan, *Chem. Phys.* **281**, 147 (2002).
- [43] Jing Guo (*private communications*).
- [44] P. S. Damle, A. W. Ghosh and S. Datta, *Chem. Phys.* **281**, 171 (2002).
- [45] C. W. J. Beenakker and H. van Houten in *Solid State Physics*, ed. by H. Ehrenreich and D. Turnbull (Academic, New York, 1991), vol. 44.
- [46] M. S. Lundstrom and Z. Ren, *IEEE Trans. El. Dev.* **49**, 133 (2002).
- [47] This mechanism of current saturation and gate modulation is the analogue of the corresponding mechanism in a ballistic MOSFET [46], and dominates over other second-order effects such as charging of the surface atoms [48] or simple Stark shifts of the molecular levels [49].
- [48] E. G. Emberly and G. Kirczenow, *Phys. Rev. B* **62**, 10451 (2000).
- [49] M. Di Ventra, S. T. Pantelides and N. D. Lang, *Appl. Phys. Lett.* **76**, 3448 (2000).
- [50] A. W. Ghosh, T. Rakshit and S. Datta, cond-mat/0212166.
- [51] D. J. Frank, R. H. Dennard, E. Nowak, P. M. Solomon, Y. Taur, H. and S. P. Wong, *IEEE* **89**, 259 (2001).
- [52] B. Yu, L. Chang, S. Ahmed, H. Wang, S. Bell, C-Y. Yang, C., Tabery, C. Ho, Q. Xiang, T-J. King, J. Bokor, C. Hu, M-R. Lin, D. Kaiser, *IEDM Tech. Digest (IEEE, Piscataway, NJ, 2002)*, 251.
- [53] B. Goebel, J. Lutzen, D. Manger, P. Moll, K. Mummler, M. Popp, U. Scheler, T. Schlosser, H. Seidl, M. Sesterhenn, S. Slesazek, S. Tegen, *IEDM Tech. Digest (IEEE, Piscataway, NJ, 2002)*, 275.